Published in final edited form as:

Cell Rep. 2021 March 09; 34(10): 108829. doi:10.1016/j.celrep.2021.108829.

Astrocyte-derived small extracellular vesicles promote synapse formation via fibulin-2-mediated TGF-β signaling

Mikin R. Patel[1,2], **Alissa M. Weaver**[1,3,4,*]

[1]Department of Cell and Developmental Biology, Vanderbilt University School of Medicine, Nashville, TN 37232, USA

[2]Department of Biological Sciences, Vanderbilt University, Nashville, TN 37232, USA

[3]Department of Pathology, Microbiology, and Immunology, Vanderbilt University Medical Center, Nashville, TN 37232, USA

[4]Lead contact

SUMMARY

Neuronal synapse formation is critical for brain development and depends on secreted factors from astrocytes. Here, we report that small extracellular vesicles (EVs) secreted from primary astrocytes, but not from neurons or C6 glioma cells, greatly enhance spine and synapse formation by primary cortical neurons. A comparative proteomics analysis of small EVs from astrocytes, neurons, and C6 glioma cells identified fibulin-2 as a promising EV cargo to regulate synaptogenesis. Treatment of cortical neurons with recombinant fibulin-2 increased the formation of spines and synapses, similar to the effect of small EVs. In addition, treatment of neurons with fibulin-2 or astrocyte-derived small EVs led to increased phosphorylation of Smad2, an indicator of TGF-β signaling. Finally, the effects of fibulin-2 and astrocyte-derived small EVs on synapse formation were reversed by inhibiting transforming growth factor β (TGF-β) signaling. These data suggest a model in which astrocyte EVs promote synapse formation via fibulin-2-mediated activation of TGF-β signaling.

Graphical Abstract

*Correspondence: alissa.weaver@vanderbilt.edu.

AUTHOR CONTRIBUTIONS

M.R.P. conducted the experiments and data analysis. M.R.P. and A.M.W. designed the experiments and wrote the manuscript.

SUPPLEMENTAL INFORMATION

Supplemental Information can be found online at https://doi.org/10.1016/j.celrep.2021.108829.

DECLARATION OF INTERESTS

A.M.W. is a member of the advisory board for *Cell Reports.* Otherwise, there are no competing interests.

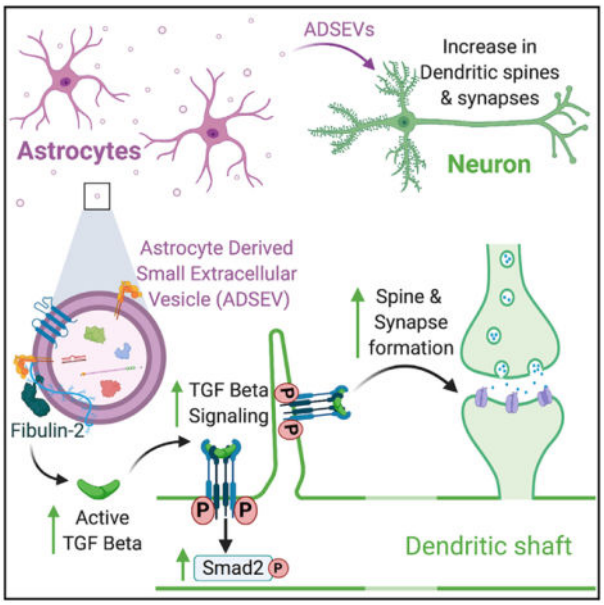

In brief

Patel and Weaver provide evidence for the function of astrocyte-derived small extracellular vesicles (SEVs) in synaptogenesis of primary cortical neurons. Astrocyte-derived SEVs carry fibulin-2 on the surface of SEVs that leads to activation of TGF-β signaling in neurons. The fibulin-2-driven TGF-β signaling drives dendritic spine and synapse formation.

INTRODUCTION

Synapses are specialized neuronal structures that consist of presynaptic and postsynaptic apposed membranes and are critical for neuronal communication, learning, and memory. Dendritic spines are protrusive postsynaptic membrane specializations with characteristic mushroom-like morphology. Formation of proper synapses occurs during early post-natal development and is highly regulated. In the past few decades, many studies have identified the importance of astrocyte to neuron communication for guiding dendritic spine and synapse formation during development (Allen, 2014; Chung et al., 2015; Jones et al., 2012; Shi et al., 2013; Ullian et al., 2001).

Astrocyte conditioned media alone can promote neuronal synapse formation, suggesting the importance of secreted molecules (Christopherson et al., 2005; Chung et al., 2015). Indeed, a number of astrocyte-secreted proteins, including thrombospondin, hevin, glypican 4, glypican 6, and the signaling molecule TGF-β1, are secreted by astrocytes and promote formation of excitatory synapses (Allen et al., 2012; Christopherson et al., 2005; Diniz et al., 2012; Eroglu et al., 2009; Singh et al., 2016; Xu et al., 2010). These and many other astrocyte-secreted proteins are often present in extracellular vesicles (EVs) (Carayon et al., 2011; Keerthikumar et al., 2015; Lee et al., 2015; Webber et al., 2010), suggesting that astrocyte-secreted EVs may participate in synaptogenesis.

EVs, including small and large EVs derived from endosomes or the plasma membrane, mediate cell-cell communication by transporting protein, lipid, and nucleic acid cargoes (Maas et al., 2017). Astrocyte-derived EVs are critical regulators of neuroprotection (Adolf et al., 2019; Hira et al., 2018; Pascua-Maestro et al., 2019; Wang et al., 2011) and neurodegeneration (Varcianna et al., 2019; Wang et al., 2012). In addition, small EVs (SEVs) isolated from ATP-treated astrocytes increase neurite length, dendrite number, and dendritic complexity (Chaudhuri et al., 2018); however, the underlying mechanism and the relationship to synapse formation is unknown.

In this study, we tested whether astrocyte-derived SEVs regulate neuronal dendritic spine and synapse formation. Treatment of cultured primary cortical neurons with astrocyte-derived SEVs, but not SEVs from neurons or C6 glioma cells, led to a significant increase in dendritic spines and synapses, at both early and late developmental stages. Quantitative proteomic analysis of SEVs identified fibulin-2 as a likely synaptogenic cargo enriched in astrocyte SEVs. Addition of recombinant human fibulin-2 to primary neurons induced spine and synapse formation to a similar extent as astrocyte-derived SEVs. Conversely, fibulin-2 knockdown astrocyte SEVs had a reduced ability to induce synaptogenesis. Investigation of the molecular mechanism indicated that the effects of astrocyte-derived SEVs and fibulin-2 are likely through receptor-mediated activation of transforming growth factor β (TGF-β) signaling.

RESULTS

Astrocyte-derived SEVs promote dendritic spine and synapse formation

To study the role of astrocyte-derived EVs in development of dendritic spines and synapses, we isolated SEVs by differential ultracentrifugation from the conditioned media of primary astrocytes that were isolated from newborn rat pups. For comparison, we used SEVs isolated from day *in vitro* 9 primary cortical neurons or from an immortalized cell line, C6 glioma, which is a glial cancer cell line with astrocytic characteristics (De Vries and Boullerne, 2010). Serum-free conditioned media was serially centrifuged at 300 × *g* for 10 min, 2,000 × *g* for 25 min, 10,000 × *g* for 30 min, and 100,000 × *g* for 18 h to pellet dead cells, cell debris, large EVs, and small EVs, respectively. Notably, very few large EVs were present in 10,000 × *g* fraction, so we were not able to analyze their effects on neurons. Due to the limited number of SEVs obtained from primary cultures, we were unable to further purify the SEVs by density gradient centrifugation. Purified SEVs were in the expected size range (30–150 nm), as measured by nanoparticle tracking analysis (Figure S1 A). Western blot analysis showed that purified SEVs were positive for common SEV markers Alix, flotillin-1, and Hsp70 and negative for the Golgi marker, GM130 (Figures S1B–S1D), suggesting minimal contamination with cell debris (Théry et al., 2018). Negative stained purified SEVs observed by transmission electron microscopy showed the expected morphology (Figure S1E).

To study the role of SEVs on spine and synapse formation, primary cortical neurons were isolated from day 19 rat embryos and cultured for 10 days before treatment with increasing doses of purified SEVs isolated from primary astrocytes, primary cortical neurons, or C6 cells. Day 10 after birth is a developmental time point when neurons begin to form spines

and synapses and are susceptible to modulation by secreted synaptogenic factors (Papa et al., 1995; Wegner et al., 2008). After 48 h (day *in vitro* 12), neurons were fixed and immunostained for the synaptic marker SV2, along with the actin stain phalloidin for visualization of spines and synapses. Treatment with astrocyte-derived SEVs led to a dose-dependent increase in the number of dendritic spines and synapses, (Figures 1A–1C). By contrast, treatment of neurons with neuronal SEVs had no effect on synapse density and slightly reduced the number of dendritic spines (Figures 1A–1C). Surprisingly, treatment of neurons with C6 glioma SEVs had no effect on spine or synapse density, despite the glial origin of this cell line (Figures 1D–1F).

We also examined whether any of the SEV preparations could affect dendritic spine formation at an earlier stage of development, day *in vitro* 5–6, when neuronal dendrites are in the process of forming actin-rich filopodia. Although many fewer dendritic spines were formed at this early developmental stage, the results were similar. Thus, astrocyte SEVs—but not the other two SEV preparations—induced neuronal dendritic spine and synapse formation (Figures S2A–S2D).

SEVs isolated from primary astrocytes are enriched with proteins distinct from cortical neuron- and C6-derived SEVs

To identify synaptogenic cargoes of astrocyte-derived SEVs, we performed isobaric tags for relative and absolute quantitation (iTRAQ) proteomic analysis on SEVs isolated from primary astrocytes, cortical neurons, and C6 glioma cells (Tables S1 and S2). Because only astrocyte SEVs induce synapse formation, we looked for proteins that were enriched in astrocyte-derived SEVs compared to the other two sets of SEVs. Analysis of the data revealed that proteins enriched in SEVs are reflective of their cells of origin (Table S2). For instance, cortical neuron SEVs were enriched with neuron-specific proteins, including neural cell adhesion molecule 1, neural cell adhesion molecule L1, synaptic vesicle glycoprotein 2a, and neuromodulin, whereas astrocyte specific proteins such as glial fibrillary acidic protein and ceruloplasmin were abundant in astrocyte-derived SEVs. We also confirmed several proteins previously identified on neuronal SEVs (Fauré et al., 2006), including beta tubulin, Hsc70, guanine nucleotide-binding protein G, and 14-3-3 proteins. Several proteins identified as >2-fold enriched in astrocyte, neuronal, or C6 SEVs by iTRAQ proteomics (Table S2) were further validated by western blot analysis and found to be highly enriched in the predicted EV sets (Figures S1F and S1G). In total, 1,237 proteins were identified in the iTRAQ analysis and 97 and 63 proteins had a respective fold change of >2 in astrocyte-derived SEVs compared to neuron SEVs and C6 SEVs. Among these, 33 proteins were >2-fold higher in astrocyte-derived SEVs compared to both neuron and C6 SEVs (Figure 2A; Table S1). Further analysis of these 33 proteins using PANTHER revealed enrichment in protein classes commonly found in EVs, including cell adhesion molecules, extracellular matrix (ECM) proteins, cytoskeletal proteins, and signaling molecules (Jimenez et al., 2019) (Figure 2B). Because astrocyte and C6 glioma SEVs are of similar glial origin and had many proteins present at similar levels in the proteomics dataset, we were able to use Benjamini-Hochberg statistics (Gobert et al., 2019; Mishra et al., 2018; Voss et al., 2015) to identify significantly enriched proteins in astrocyte-derived SEVs compared to C6 SEVs (see STAR methods). Based on this analysis, 12 out of the 33 proteins were significantly enriched in

astrocyte-derived SEVs compared to C6 SEVs (Figure 2C). We prioritized these 12 proteins as top candidates to promote synapse formation.

Fibulin-2 is a synaptogenic cargo present in astrocyte SEVs

ECM proteins and TGF-β signaling are known to regulate synapse formation and plasticity (Barros et al., 2011; Diniz et al., 2012; Levy et al., 2014; Song and Dityatev, 2018). In our proteomics analysis, we identified the ECM protein, fibulin-2, as significantly enriched in astrocyte SEVs compared to C6 (>6-fold) and neuronal (>5-fold) SEVs (Figure 2C). Fibulin-2 has also been shown to promote TGF-β activation (Khan et al., 2016) and to regulate TGF-β1-induced differentiation of adult neural stem cells into neurons (Radice et al., 2015). Based on these studies, we investigated whether fibulin-2 might account for the activity of astrocyte SEVs in promoting spine and synapse density.

Western blot analysis confirmed that fibulin-2 is present in astrocyte cell lysates and SEVs but is undetectable in cell lysates and SEVs from cortical neurons or C6 glioma cells (Figures 3A and S2E). To study its role in synapse formation, recombinant human fibulin-2 was either coated on coverslips before plating neurons or added into the media of cortical neurons on day 10 at 0.5 or 2 μg/mL concentrations. After 48 h, the neurons were analyzed for dendritic spines and synapses (Figure 3B). For all conditions, except for 0.5 μg/mL fibulin-2 coating, there was a significant increase in spine and synapse density (Figures 3C and 3D). Because 2 μg/mL of fibulin-2 added to the media was the most effective condition, we used it for subsequent experiments.

To test the function of EV-carried fibulin-2 in synaptogenesis, astrocytes were transiently transfected with small interfering RNA (siRNA) against fibulin-2 or non-targeting control. Fibulin-2 knockdown was confirmed by western blot analysis in cell lysates at the times of conditioning and collection of conditioned media, 48 and 72 h post-transfection, respectively (Figure S2F), and in purified SEVs (Figures 3E and 3F). Consistent with fibulin-2 being a key synaptogenic EV cargo, treatment of neurons with fibulin-2-knockdown astrocyte-derived SEVs induced significantly fewer spines and synapses than control SEVs (Figures 3G–3I).

Astrocyte-derived SEVs and fibulin-2 activate TGF-β signaling to increase spine and synapse formation

We hypothesized that fibulin-2 carried by SEVs induces TGF-β signaling. Notably, whereas TGF-β1, TGF-β2, and TGF-β3 were present in our proteomics data, they were not enriched in SEVs derived from astrocytes compared to C6 cells (Table S2), suggesting that any differences would be due to accessory factors. To determine whether astrocyte SEVs or fibulin-2 can induce TGF-β signaling, cortical neurons were treated with SEVs purified from astrocytes, cortical neurons, or C6 cells, 2 μg/mL recombinant fibulin-2, or 10 ng/mL TGF-β1 as a positive control. As an additional control, treatments were performed in the presence or absence of the TGF-β signaling inhibitor, SB431542 (SB). After 1 h, cell lysates were analyzed by western blot for levels of phosphorylated (pSmad2) and total Smad2. Consistent with our hypothesis, neurons treated with TGF-β1, fibulin-2, or astrocyte SEVs had significantly increased pSmad2 levels compared to untreated control neurons (Figures 4A

and 4B). pSmad2 levels were unchanged by treatment with neuronal or C6 SEVs. Smad2 phosphorylation was inhibited in all conditions in which 10 μM SB was added.

To test whether TGF-β signaling is important for the synaptogenic effects of astrocyte SEVs and fibulin-2, day *in vitro* 10 cortical neurons were treated with astrocyte SEVs, 2 μg/mL recombinant fibulin-2, or 10 ng/mL TGF-β1 for 48 h in the presence or absence of 10 μM SB. Analysis of SV2 immunostaining in the cortical neurons revealed that TGF-β signaling inhibition indeed blocks the phenotypic effects of astrocyte SEVs and fibulin-2 (Figures S3A–S3D). Furthermore, recombinant TGF-β mimicked the synaptogenic effect of astrocyte SEVs and fibulin-2. Similar effects of astrocyte SEVs and TGF-β were likewise observed for early stage day *in vitro* 6 neurons (Figures S3E and S3F, fibulin-2 was not tested).

In the baseline control condition, pSmad2 and synaptogenesis were significantly reduced by 10 μM SB. Therefore, lower concentrations of SB were tested to identify concentrations that only inhibit TGF-β1-induced Smad2 phosphorylation (Figure S3G). In addition, we used a second method to inhibit TGF-β signaling, with a pan-TGFβ-neutralizing antibody (Figure S3H). We identified 2.5 μM SB or 10 μg/mL pan-TGFβ-neutralizing antibody to be optimal concentrations to inhibit TGFβ1-induced Smad2 phosphorylation (Figures S3G and S3H). Using these conditions, we found that neuronal dendritic spines and synapses induced by TGF-β1, fibulin-2, or astrocyte SEVs were inhibited by 2.5 μM SB or 10 μg/mL pan-TGFβ-neutralizing antibody (Figures 3C and 3D). Dendritic spine and synapse density were also examined using PSD95, a postsynaptic marker, and uptake of the lipophilic dye FM4-64, a marker for synaptic activity. As with SV2 and phalloidin staining, treatment of cortical neurons with TGF-β1, fibulin-2, and astrocyte SEVs induced an increase in spines and synapses positive for PSD95 and FM4-64 (Figures S4A–S4F).

Activation of TGF-β signaling in cortical neurons by astrocyte-derived SEVs could be receptor-mediated or require SEV internalization. To help distinguish these possibilities, neurons were treated with TGF-β1, fibulin-2, or astrocyte SEVs to measure Smad2 phosphorylation at different time points. For all treatments, pSmad2 levels increased at 15 min and 1 h, after which it declined (Figure 4E). To further explore the mechanism, pSmad2 levels were measured in neurons treated with TGF-β1, fibulin-2, or astrocyte SEVs for 1 h in the absence or presence of the endocytosis inhibitor, Dynasore. Dynasore treatment had a small but significant inhibitory effect on TGF-β1, fibulin-2, or astrocyte SEV-induced pSmad2 levels. These data suggest that endocytosis enhances but is not necessary for the induction of TGF-β signaling by astrocyte SEVs and fibulin-2. The ability of Dynasore to inhibit endocytosis in our system was confirmed by observing internalization of fluorescent transferrin by neurons (Figure S4G). The rapid activation of TGF-β signaling by astrocyte SEVs and fibulin-2 (Figure 4E), together with the small effect of Dynasore, suggest that the signaling is likely to be primarily receptor-mediated at the cell surface. To activate extracellular TGF-β, fibulin-2 should be present on the outside of astrocyte SEVs. Indeed, using a dot-blot assay in which EVs are permeabilized with 0.1% Tween to reveal internal cargoes (Lai et al., 2015; McKenzie et al., 2016; Sung and Weaver, 2017), we detect the cytoplasmic protein Alix mainly in the presence of detergent. However, fibulin-2 was detected with equivalent intensity in the absence or presence of detergent, indicating its localization to the outside of SEVs (Figure S4H).

DISCUSSION

Secreted factors from astrocytes are critical for neuronal development and function. We found that astrocyte-derived SEVs promote spine and synapse formation in primary cultured neurons. Using a quantitative proteomic approach, we identified fibulin-2 as strongly enriched in astrocyte SEVs compared to neuronal and C6 glioma SEVs. Follow-up experiments revealed that recombinant fibulin-2 promotes and that fibulin-2 knockdown SEVs are deficient in inducing synaptogenesis. Both astrocyte SEV- and fibulin-2-dependent spine and synapse formation depend on TGF-β signaling. The rapid induction of TGF-β signaling by SEVs and fibulin-2, the presence of fibulin-2 on the outside of SEVs, and the relative insensitivity to endocytosis inhibition suggest a model in which fibulin-2 carried by astrocyte SEVs augments TGF-β signaling at the cell surface of neurons.

Astrocyte EVs can regulate neurite length and dendritic complexity (Chaudhuri et al., 2018; Luarte et al., 2020; You et al., 2019). Although treatment of the astrocytes with IL-1β was shown to diminish the neurite-inducing activity of the secreted EVs, via EV-carried miRNAs, no mechanism was investigated for the positive effects of astrocyte EVs on neuronal outgrowth. In our study, we specifically focused on whether astrocyte SEVs induce synapse formation, using SV2, PSD95, and FM-464 staining as readouts. Because increased dendritic complexity typically accompanies synapse formation, it seems possible that fibulin-2 carried by SEVs may drive some of the positive effects of astrocyte SEVs on neuronal dendritic specialization. If so, the downregulation of such activities by SEV-carried miRNAs speaks to the molecular complexity of SEVs secreted by cells and the multiple modes by which SEVs alter the phenotypes of recipient cells.

Although fibulin-2 is an ECM molecule, many of its biologic effects appear related to regulation of TGF-β activity. Fibulin-2 has been shown to be essential for TGF-β-mediated cardiac hypertrophy and fibrosis and to promote TGF-β-signaling (Khan et al., 2016; Zhang et al., 2014). In one of these studies, addition of recombinant fibulin-2 to fibulin-2 knockout cells was able to partially rescue Smad2 phosphorylation, suggesting that fibulin-2 may directly activate TGF-β signaling (Khan et al., 2016). Apart from cardiac fibroblasts, fibulin-2 is also required for TGF-β1 to increase neurogenesis in adult neural stem cells (Radice et al., 2015).

TGF-β1 is a synaptogenic factor secreted by astrocytes that increases excitatory synapse formation (Diniz et al., 2012, 2014) and protects neurons against spine and synapse loss induced by amyloid beta oligomers (Diniz et al., 2017). Consistent with our finding that TGF-β1 signaling is important for astrocyte SEV-mediated spine and synapse formation, mice deficient for TGF-β1 in the CNS display a significant reduction in dendritic spine density in pyramidal cells of hippocampal slices prepared from 21-day-old mice (Koeglsperger et al., 2013). By contrast, in a mouse model of depression, increased fibulin-2 and TGF-β1 expression were associated with decreased dendritic spines and knockdown of fibulin-led to a partial rescue in dendritic spine density (Tang et al., 2019). Further study will be required to understand why fibulin-2 and/or TGF-β signaling has divergent effects on dendritic specializations in adult disease versus in developing neurons.

TGF-β1 is released from cells as a latent complex and requires activation to exert its functions. Both active and inactive forms of TGF-β1 are present in EVs (Shelke et al., 2019; Webber et al., 2010). Inactive TGF-β1 present in EVs can be activated and can induce prolonged signaling in recipient cell endosomes (Shelke et al., 2019). However, astrocyte SEVs did not induce prolonged TGF-β signaling in neurons. Furthermore, astrocyte SEV-induced TGF-β signaling was only slightly diminished by inhibition of endocytosis, suggesting that most of the EV-induced TGF-β signaling occurred at the cell surface. In our proteomics data, we identified multiple TGF-β isoforms and latent TGF-β binding proteins present in astrocyte SEVs; however, none of these proteins were enriched in astrocyte SEVs compared to C6 EVs. We also did not detect the ECM protein thrombospondin-1 that can activate TGF-β1 by direct interaction with the latent complex (Murphy-Ullrich and Poczatek, 2000; Yu et al., 2008). The molecular mechanism by which fibulin-2 activates TGF-β signaling remains unknown; however it has been postulated that fibulin-2 may either release active TGF-β1 from the latent complex by facilitating cleavage or increase TGF-β bioavailability by competing with a latent TGF-β binding protein for fibrillin-1 binding (Costanza et al., 2017; Onoet al., 2009). Our data suggest that EVs are an important platform for this process.

For our proteomics analysis, we used a statistical comparison between astrocyte and C6 SEV cargo proteins to narrow our potential candidates to twelve proteins. Of these twelve proteins, none were previously shown to directly regulate synaptogenesis. However, fibulin-2 had been reported to promote TGF-β1 signaling, which has known function in synaptogenesis (Diniz et al., 2012, 2014). Furthermore, fibulin-2 expressed by astrocytes is known to be important for neurogenesis and CNS repair (Radice et al., 2015; Schaeffer et al., 2018). Therefore, we followed up on fibulin-2 as our top candidate. Because we did not perform replicate proteomics experiments, more experiments would be required to make firm conclusions about large-scale differences between the SEV samples. However, we note that we were able to easily validate differences in the levels of selected cargoes by western blot analysis and also successfully identified fibulin-2 as a key synaptogenic cargo.

Another limitation of our study is that it was all carried out *in vitro,* albeit with primary cultures. In the brain, EV secretion from multiple cell types may lead to complex regulation of signaling pathways involved in spine and synapse formation. Fibulin-2 has been shown to regulate spinal nerve outgrowth in a chick embryo model and to be expressed at higher levels in reactive astrocytes at the lesion site in a CNS injury mouse model, suggesting functions in CNS repair and plasticity (Schaeffer et al., 2018). However, the *in vivo* functions of fibulin-2 and astrocyte SEVs in synapse formation during neuronal development remain to be demonstrated. We also did not investigate what pathways may regulate secretion of fibulin-2-carrying EVs from astrocytes. Although IL-1β treatment of astrocytes is known to alter EV biogenesis and dendritic complexity, whether it affects the number of fibulin-2-carrying EVs released from astrocytes is currently unknown (Chaudhuri et al., 2018; Dickens et al., 2017).

Fibulin-2 can bind to other ECM proteins, including fibronectin, fibrillin-1, and some heparin sulfate proteoglycans (Sasaki et al., 1995; Timpl et al., 2003), which were also present on astrocyte SEVs according to our iTRAQ proteomics data. Therefore, it is

conceivable that fibulin-2 may be associated with many of its known binding partners on SEVs. Because adhesion molecules may target SEVs to specific sites, it is also possible that ECM associated with SEVs may serve multiple purposes, including binding recipient cells and delivery of signaling molecules.

In summary, we identified a distinct role of primary astrocyte-derived SEVs in the development of dendritic spines and synapses via activation of TGF-β signaling. Our proteomics analysis identified fibulin-2 as a key astrocyte SEV cargo that promotes TGF-β signaling and drives synaptogenesis.

STAR★METHODS

RESOURCE AVAILABILITY

Lead contact—Further information and requests for resources and reagents should be directed to, and will be fulfilled by, the Lead Contact, Alissa M. Weaver (alissa.weaver@vanderbilt.edu).

Materials availability—This study did not generate new unique reagents.

Data and code availability—The datasets supporting the current study have not been deposited in a public repository yet because all datasets are either supplied as a supplement (proteomics) or are available from the corresponding author on request (images).

EXPERIMENTAL MODEL AND SUBJECT DETAILS

Primary neuron and astrocyte cultures and cell lines—Primary rat cortical neurons were isolated from the brains of embryos from 19 day pregnant Sprague Dawley rats. Cortices from both cerebral hemispheres of the E19 rat embryo brains were chopped into small pieces, incubated in 0.05% Trypsin at 37°C for 15 min and washed three times with Hank's Balanced Salt Solution (HBSS) without calcium and magnesium. After the final wash, cells were triturated with a sterile glass pipet and plated on coverslips in dishes at the desired density. Neurons were plated either on 18 or 25mm glass coverslips at low density (300,000 in 60mm culture dishes) for fixed cell analysis or at high density (2.6 million in 100mm culture dishes) for exosome isolation, both coated with 50 μg/ml poly-D-lysine. After 4 h, neurons plated at low density on coverslips were transferred to 60mm dishes containing > 80% confluent primary astrocytes, using wax dots to separate the coverslips from the dish surface. The DNA synthesis inhibitor Cytosine Arabinoside (Ara-C) was added on day *in vitro* (*DIV*) 2 to a final concentration of 5 μM to inhibit glia growth.

Primary astrocytes were obtained from postnatal P1-P2 day rats. Both cerebral hemispheres were dissected from each P1-P2 rat and meninges were removed. Collected tissues were chopped into fine pieces and incubated in 0.25% Trypsin, 0.1% DNase I at 37°C for 15 min with occasional swirling. The supernatant containing dissociated cells was passed through a 70 μm nylon mesh cell strainer into to a 50ml conical tube containing horse serum to make final concentration of 10% horse serum and centrifuged at 200×g for 6 min to pellet the cells. The supernatant was carefully removed and cells were resuspended in Minimum Essential Medium containing 0.6% glucose, 10% horse serum, 1% Penicillin-Streptomycin

and plated in T75 flasks at a concentration of 5–10 × 10^6 cells per flask. After 24 h, flasks were tapped from the side to detach any microglia and the media was replaced. Thereafter, the media was replaced twice a week until the cells reached 100% confluence. All animal procedures were performed in compliance with IACUC approved protocol M1800027-00 at Vanderbilt University. The C6 glioma cell line was kindly provided by Dr. James G. Patton at Vanderbilt University. C6 glioma cells were cultured in F-12K media (ThermoFisher) supplemented with 10% Horse serum, 2.5% Fetal bovine serum and 1% Penicillin-Streptomycin.

METHOD DETAILS

SEV isolation and characterization—For neuronal exosomes, day *in vitro* (*DIV*) 9 cortical neurons cultured at high density (2.6 million in 100 mm culture dishes) were washed three times with HBSS. After the final wash, HBSS was replaced with 4 mL Neurobasal media per 100 mm dish. Neurobasal media does not contain serum but contains growth factors. Neurobasal conditioned media was collected after 4 h incubation. For astrocyte SEVs, primary astrocytes grown to 90%–100% confluency were washed three times with HBSS and then conditioned with neurobasal media for 24 hr. For C6 Glioma cells, 8 million cells were plated per T225 flask and cultured for 48 h in F-12K media containing 10% horse serum and 2.5% FBS to reach 80% confluence. After that, cells were washed three times with prewarmed 1x PBS and cultured in serum free F-12K media for 48 hr. Conditioned media from all cell types was collected and processed for differential ultracentrifugation. Briefly, conditioned media was centrifuged sequentially at 300×g for 10 min, 2000×g for 25 min in a tabletop centrifuge, and 10,000×g for 30min in a Type 45 Ti ultracentrifuge rotor (Beckman) to remove live cells, cell debris and micro-vesicles (MVs), respectively. The supernatant from the 10,000×g spin was centrifuged at 100,000×g for 18 hr in a Type 45 Ti rotor to obtain SEVs. The 100,000×g SEV-containing pellets were resuspended in 3 mL sterile cold PBS and repelleted at 100,000×g for 4 hr in a TLA110 rotor. SEVs were analyzed for size and number by nanoparticle tracking (ZetaView, ParticleMetrix) and for common SEV markers by western blotting (See also Figure S2).

Transmission Electron Microscopy—Purified SEVs reconstituted in 20 mM HEPES buffer were added on glow-discharged formvar carbon film-coated grids in 10 μL volume for 1 min at room temperature. Subsequently, grids were stained with 2% uranyl acetate for 30 s and were allowed to air dry. Grids were imaged using a Philips/FEI T-12 transmission electron microscope at 21000x magnification.

iTRAQ sample preparation and Proteomics—iTRAQ proteomics analysis was performed on purified neuronal, astrocyte or C6 glioma SEVs. To prepare samples, SEVs were washed three times with 1x PBS to remove any soluble protein contaminants. SEV samples in PBS at equal protein concentration were lysed 1:1 with 2X lysis buffer (200 mM TEAB, 600 mM NaCl, 4% NP-40, 1% Sodium Deoxycholate) and incubated in a cold sonicating water bath (Bioruptor) for 15 min. The samples were then centrifuged at 21,100×g for 30 min at 4°C and the supernatants containing soluble protein were carefully collected for iTRAQ proteomics analysis.

Protein samples were precipitated with ice-cold acetone overnight at −20°C. Following precipitation, samples were centrifuged at 18,000×g at 4°C, and precipitates were washed with cold acetone, dried, and reconstituted in 8M urea in 250 mM TEAB (pH 8.0). Samples were reduced with TCEP, alkylated with MMTS, diluted with TEAB to obtain a final solution containing 2M urea, and digested with sequencing-grade trypsin overnight. To facilitate quantitative analysis, peptides were labeled with iTRAQ reagents according to the manufacturer's instructions (SCIEX). Labeling reagent was reconstituted in ethanol such that each protein sample was labeled at a final concentration of 90% ethanol, and labeling was performed for 2 hours. The resulting peptides were the desalted by a modified Stage-tip method (Jimenez et al., 2019). Peptides were reconstituted and analyzed using a MudPIT LC MS/MS method (Jimenez et al., 2019). Following each salt pulse delivered by the autosampler, peptides were gradient-eluted from the reverse analytical column at a flow rate of 350nL/min. Mobile phase solvents consisted of 0.1% formic acid, 99.9% water (solvent A) and 0.1% formic acid, 99.9% acetonitrile (solvent B). For the peptides from the first 11 SCX fractions, the reverse phase gradient consisted of 2%–50% B in 83 min, 50% B for 2 minutes, and a 10 min equilibration at 2% B. For the last 2 SCX-eluted peptide fractions, the peptides were eluted from the reverse phase analytical column using a gradient of 2%–98% B in 83 min, followed by 98% B for 2 minutes, and a 10 min equilibration at 2% B. Peptides were introduced via nano-electrospray into a Q Exactive Plus mass spectrometer (Thermo Scientific). The Q Exactive Plus was operated in the data-dependent mode acquiring HCD MS/MS scans (R = 17,500) after each MS1 scan on the 15 most abundant ions using an MS2 target of 1×10^5 ions. The HCD-normalized collision energy was set to 30, dynamic exclusion was set to 30 s, and peptide match and isotope exclusion were enabled. Mass spectra were processed using the Spectrum Mill software package (version B.04.00) (Agilent Technologies) with similar parameters as described in Jimenez et al. (2019) and were searched against a database containing the *Rattus norvegicus* subset of the UniprotKB protein database (https://www.uniprot.org). Search parameters included: trypsin enzyme specificity, ± 20 ppm (HCD) product mass tolerance, and fixed modifications including MMTS alkylation of cysteines and iTRAQ labeling of lysines and peptide N-termini. Oxidation of methionine was allowed as a variable modification. Autovalidation was performed such that the maximum target-decoy-based false-discovery rate (FDR) was set to 1.0%. To obtain iTRAQ protein ratios, the median was calculated for all peptides assigned to each protein.

For statistical analysis of iTRAQ protein ratios, log2 protein ratios were fit to a normal distribution using non-linear (least-squares) regression. The calculated mean derived from the Gaussian fit was used to normalize individual log2 ratios for each quantified protein. The normalized log2 ratios were then fit to a normal distribution, and the mean and standard deviation values derived from the Gaussian fit of the normalized ratios were used to calculate p values using Z score statistics. Subsequently, p values were corrected for multiple comparisons by the Benjamini-Hochberg (BH) method. Proteins with a BH FDR $p < 0.05$ were defined as significantly changed. Proteins that were identified as Uncharacterized proteins were searched through panther and UniProt databses manually by entering the accession number. Proteins with normalized fold change of > 2 in ADSEVs compared to CNSEVs or C6SEVs were identified. PANTHER (www.pantherdb.org) was used to identify

protein classes of the 33 proteins enriched in ADSEVs compared to both CNSEVs and C6SEVs.

Western Blot Analysis—To prepare cell lysates, cells were washed rapidly once with 1x HBSS and then lysed using 10 mM Tris pH 7.4, 1% SDS. Protein concentrations of total cell lysates were measured using the Pierce BCA assay. For SEVs, a MicroBCA Protein Assay Kit (Pierce) was used to determine protein concentration. Samples loaded by equal protein concentration were resolved on 8% SDS-PAGE gels and transferred to nitrocellulose membranes. Ponceau S stain was used to confirm proper protein transfer onto membranes, before washing 3 times with 1X TBS buffer and blocking in 5% milk in 1X TBST. Primary antibodies were diluted in 5% milk (TSG101 1:1000, Flotillin-1 1:1000, GM130 1:1000, Alix 1:1000, Hsp70 1:1000, Fibulin-2 1:2000, Smad2 1:5000) or 5% BSA (pSmad2 1:5000) and HRP-conjugated secondary antibodies were diluted 1:10,000 in 5% milk in TBST before developing with ECL reagent and imaging with an Amersham 680 imager. ImageStudioLite (LI-COR version 5.2.5) was used for densitometry analysis.

Dot blot assay—Astrocyte-derived SEVs at different concentrations in 10 μL final volume were dotted on nitrocellulose membranes and allowed to air dry for 1 h at room temperature. Membranes were then blocked with 5% milk in TBS in the absence (TBS) or presence of 0.1% (v/v) Tween-20 (TBST) for 1 h at room temperature. Subsequently, membranes were incubated with primary antibodies against fibulin-2 or Alix and then HRP conjugated secondary antibodies in 5% milk with TBS or TBST followed by imaging with Amersham 680 imager.

Treatment of primary neurons—Primary neurons on glass coverslips at low density (300,000 in 60 mm culture dishes) were co-cultured with astrocytes in 60 mm dishes. To find a concentration range of SEVs to test, we estimated the SEV secretion rate for neurons, astrocytes, and C6 cells to be ~8 SEVs/cell/h based on the total concentration of purified SEVs measured by NTA divided by the number of cells and the conditioning time. We estimated that ~400 EVs/cell would be the approximate number secreted over 48 h and tested a concentration range above and below that amount (200, 1000, and 2000 SEVs/neuron) for experiments. For experiments in Figures 1 and S2, neurons in co-cultures with astrocytes were treated with increasing doses of SEVs. For all other experiments, neurons were transferred to 12-well plates on *DIV* 5 or *DIV* 10 with 1 mL conditioned media per well from the home dish and treated for 24 h (*DIV5–DIV6*) or 48 h (*DIV10–DIV12*). Neurons were then fixed and stained with phalloidin oranti-SV2 antibody on *DIV6* (early stage) or *DIV12* (late stage) to examine spines and synapses. For analysis of phosphorylated Smad2, neurons plated in poly-D-lysine coated 12-well plates at high density (500,000 per well) were treated on *DIV10*, first with 10 μm SB4315242 or diluent for 5 min and then with 10 ng/ml TGF-β1,2 μg/ml recombinant human fibulin-2, or purified SEVs from cortical neurons, astrocytes or C6 cells for 1 h.

Transfection of primary astrocytes—Astrocytes were transfected in 6-well plates with SMARTpool siRNAs (Dharmacon) against fibulin-2 or non-targeted control using X-tremeGENE™ siRNA transfection reagent (Millipore Sigma) according to the

manufacturer's instructions. Briefly, astrocytes were grown at ~80%–90% confluency in 6-well plates. Before transfection, media was changed to antibiotic-free glia culture media. For transfection of each well, 2.5 μL of 100 μM siRNAs was diluted in 125 μL of serum free MEM in one tube and 25 μL of transfection reagent was added to 100 μL of serum free MEM in another tube. The resulting mixture from both tubes was combined immediately, incubated at room temperature for 20 min and added dropwise to the cells. 48 h post transfection, the cells were washed three times with HBSS and conditioned with neurobasal media for 24 h. Conditioned media was subjected to differential ultracentrifugation for isolation of purified SEVs.

Immunocytochemistry—Neurons at room temperature were fixed in 4% paraformaldehyde in PBS for 15 mins, for SV2 staining, or 3 mins followed by 10 min incubation with ice cold methanol for PSD95 staining. Neurons were then permeabilized with 0.2% Triton X-100 in PBS for 3 min, then incubated for 1 h with 20% goat serum to block non-specific antibody binding at room temperature. Alexa Fluor 488 phalloidin, anti-PSD95 and anti-SV2 antibody were diluted at 1:1000 in 5% goat serum and incubated overnight with the neurons at 4°C before washing and incubating with 1:1000 anti-mouse Alexa Fluor 647 antibody for 45 mins at room temperature. Coverslips were washed in PBS, then rinsed in deionized distilled water before mounting on glass slides with Aqua-Poly/Mount.

FM4-64 labeling—A fixable analog of FM4-64FX (Invitrogen) was diluted to 5 μg/ml working solution in high K^+ solution (72mM NaCl, 50mM KCl, 1mM NaH_2PO_4, 26mM $NaHCO_3$, 1.8mM $CaCl_2$, 0.8mM $MgSO_4$, 11mM glucose and 20mM HEPES, pH-7.35). Day 12 neurons were incubated with FM4-64FX for 1 min at room temperature and washed three times using HBSS without magnesium or calcium. Neurons were then fixed with 4% PFA for 15 min and stained with phalloidin before mounting on glass slides for imaging.

Dynasore treatment and transferrin internalization assay—Day 10 neurons were incubated at 37°C with 100 μM Dynasore in neurobasal media for 30 mins. Neurons were then incubated with fluorescent transferrin (Molecular Probes) in neurobasal media with or without 100 μM Dynasore at final concentration of 25 μg/ml for 2 mins at room temperature followed by 30 min incubation at 37°C. Next, neurons were washed three times with neurobasal media with or without 100 μM Dynasore followed by fixing with 4% PFA for 15 min and staining with phalloidin.

Microscopy and image analysis—For most experiments, neurons were imaged on a Nikon A1R HD confocal microscope equipped with an Apo TIRF 60x/1.49 NA oil immersion lens. Images were acquired using NIS-Elements software. For some experiments (Figures 1A and S3A), neurons were imaged using MetaMorph software on a Quorum Wave-FX Yokogava CSU-X1 spinning disk confocal system with a Nikon Eclipse Ti microscope equipped with an Apo TIRF 60x/1.49 NA oil immersion lens. To examine dendritic spine and synapse density, 12 to 15 images of primary or secondary dendrites were acquired for each experiment for a total of 36–45 images from three independent experiments. Images were analyzed manually for dendritic spine and synapse density using

either MetaMorph or NIS-Elements software to trace dendrite length. The scale slider in MetaMorph or the histogram scale in NIS-Elements was used to reduce background and improve signal to aid in visualization of SV2 co-localization in phalloidin/SV2 overlay. Any scale changes were made equally across the whole image. Dendritic spines were defined as phalloidin-positive protrusions co-localized with the presynaptic marker SV2 while synapses were defined as SV2 puncta co-localized to both dendritic protrusions and dendritic shafts. For all images shown in figures, Fiji (ImageJ Version 2.0) was used to adjust the brightness and contrast display levels across the whole image for visualization purposes and all images were cropped to the same size (40 μm × 15 μm) in Fiji.

QUANTIFICATION AND STATISTICAL ANALYSIS

GraphPad Prism version 8 was used to analyze and plot all data. The Mann-Whitney test was used to calculate the *p-value* between each set of conditions. The data for dendritic spine and synapse densities from three independent experiments were combined and plotted as box and whiskers plots, where the bar indicates the median with interquartile range and all data points are shown. Image-StudioLite (LI-COR version 5.2.5) was used for densitometry analysis of western blots. The relative density of bands was measured as the signal from the same area for each band, with background correction. For graphs, pSmad2 levels were normalized to total Smad2 levels. The adjusted density was then calculated by normalizing all treatment conditions to control. A Z-test was performed to statistically compare each condition with control.

Supplementary Material

Refer to Web version on PubMed Central for supplementary material.

ACKNOWLEDGMENTS

iTRAQ proteomics was performed in the Mass Spectrometry Research Center (MSRC) Proteomics Core Laboratory at Vanderbilt University, with the help of Kristie Rose. Transmission electron microscopy was performed with the help of Evan Krystofiak at the Vanderbilt Cell Imaging Shared Resource (CISR). We thank members of the Weaver Laboratory and Dr. James G. Patton for feedback. This work was funded by NIH (R01 GM117916).

REFERENCES

Adolf A, Rohrbeck A, Münster-Wandowski A, Johansson M, Kuhn HG, Kopp MA, Brommer B, Schwab JM, Just I, Ahnert-Hilger G, and Höltje M (2019). Release of astroglial vimentin by extracellular vesicles: Modulation of binding and internalization of C3 transferase in astrocytes and neurons. Glia 67, 703–717. [PubMed: 30485542]

Allen NJ (2014). Astrocyte regulation of synaptic behavior. Annu. Rev. Cell Dev. Biol 30, 439–63. [PubMed: 25288116]

Allen NJ, Bennett ML, Foo LC, Wang GX, Chakraborty C, Smith SJ, and Barres BA (2012). Astrocyte glypicans 4 and 6 promote formation of excitatory synapses via GluA1 AMPA receptors. Nature 486, 410–414. [PubMed: 22722203]

Barros CS, Franco SJ, and Müller U (2011). Extracellular matrix: functions in the nervous system. Cold Spring Harb. Perspect. Biol 3, a005108. [PubMed: 21123393]

Carayon K, Chaoui K, Ronzier E, Lazar I, Bertrand-Michel J, Roques V, Balor S, Terce F, Lopez A, Salomé L, and Joly E (2011). Proteolipidic composition of exosomes changes during reticulocyte maturation. J. Biol. Chem 286, 34426–34439. [PubMed: 21828046]

Chaudhuri AD, Dastgheyb RM, Yoo SW, Trout A, Talbot CC Jr., Hao H, Witwer KW, and Haughey NJ (2018). TNFα and IL-1β modify the miRNA cargo of astrocyte shed extracellular vesicles to regulate neurotrophic signaling in neurons. Cell Death Dis. 9, 363. [PubMed: 29507357]

Christopherson KS, Ullian EM, Stokes CC, Mullowney CE, Hell JW, Agah A, Lawler J, Mosher DF, Bornstein P, and Barres BA (2005). Thrombospondins are astrocyte-secreted proteins that promote CNS synaptogenesis. Cell 120, 421–433. [PubMed: 15707899]

Chung WS, Allen NJ, and Eroglu C (2015). Astrocytes Control Synapse Formation, Function, and Elimination. Cold Spring Harb. Perspect. Biol 7, a020370. [PubMed: 25663667]

Costanza B, Umelo IA, Bellier J, Castronovo V, and Turtoi A (2017). Stromal Modulators of TGF-β in Cancer. J. Clin. Med 6, 7.

De Vries GH, and Boullerne AI (2010). Glial cell lines: an overview. Neurochem. Res 35, 1978–2000. [PubMed: 21127972]

Dickens AM, Tovar-Y-Romo LB, Yoo SW, Trout AL, Bae M, Kanmogne M, Megra B, Williams DW, Witwer KW, Gacias M, et al. (2017). Astrocyte-shed extracellular vesicles regulate the peripheral leukocyte response to inflammatory brain lesions. Sci. Signal 10, eaai7696. [PubMed: 28377412]

Diniz LP, Almeida JC, Tortelli V, Vargas Lopes C, Setti-Perdigão P, Stipursky J, Kahn SA, Romão LF, de Miranda J, Alves-Leon SV, et al. (2012). Astrocyte-induced synaptogenesis is mediated by transforming growth factor β signaling through modulation of D-serine levels in cerebral cortex neurons. J. Biol. Chem 287, 41432–41445. [PubMed: 23055518]

Diniz LP, Matias IC, Garcia MN, and Gomes FC (2014). Astrocytic control of neural circuit formation: highlights on TGF-beta signaling. Neurochem. Int 78, 18–27. [PubMed: 25125369]

Diniz LP, Tortelli V, Matias I, Morgado J, Bérgamo Araujo AP, Melo HM, Seixas da Silva GS, Alves-Leon SV, de Souza JM, Ferreira ST, et al. (2017). Astrocyte Transforming Growth Factor Beta 1 Protects Synapses against Aβ Oligomers in Alzheimer's Disease Model. J. Neurosci 37, 67976809.

Eroglu C, Allen NJ, Susman MW, O'Rourke NA, Park CY, Ozkan E, Chakraborty C, Mulinyawe SB, Annis DS, Huberman AD, et al. (2009). Gabapentin receptor alpha2delta-1 is a neuronal thrombospondin receptor responsible for excitatory CNS synaptogenesis. Cell 139, 380–392. [PubMed: 19818485]

Fauré J, Lachenal G, Court M, Hirrlinger J, Chatellard-Causse C, Blot B, Grange J, Schoehn G, Goldberg Y, Boyer V, et al. (2006). Exosomes are released by cultured cortical neurones. Mol. Cell. Neurosci 31, 642–648. [PubMed: 16446100]

Gobert AP, Latour YL, Asim M, Finley JL, Verriere TG, Barry DP, Milne GL, Luis PB, Schneider C, Rivera ES, et al. (2019). Bacterial Pathogens Hijack the Innate Immune Response by Activation of the Reverse Trans-sulfuration Pathway. MBio 10, e02174–19. [PubMed: 31662455]

Hira K, Ueno Y, Tanaka R, Miyamoto N, Yamashiro K, Inaba T, Urabe T, Okano H, and Hattori N (2018). Astrocyte-Derived Exosomes Treated With a Semaphorin 3A Inhibitor Enhance Stroke Recovery via Prostaglandin D_2 Synthase. Stroke 49, 2483–2494. [PubMed: 30355116]

Jimenez L, Yu H, McKenzie AJ, Franklin JL, Patton JG, Liu Q, and Weaver AM (2019). Quantitative Proteomic Analysis of Small and Large Extracellular Vesicles (EVs) Reveals Enrichment of Adhesion Proteins in Small EVs. J. Proteome Res 18, 947–959. [PubMed: 30608700]

Jones EV, Cook D, and Murai KK (2012). A neuron-astrocyte co-culture system to investigate astrocyte-secreted factors in mouse neuronal development. Methods Mol. Biol 814, 341–352. [PubMed: 22144317]

Keerthikumar S, Gangoda L, Liem M, Fonseka P, Atukorala I, Ozcitti C, Mechler A, Adda CG, Ang CS, and Mathivanan S (2015). Proteogenomic analysis reveals exosomes are more oncogenic than ectosomes. Oncotarget 6, 15375–15396. [PubMed: 25944692]

Khan SA, Dong H, Joyce J, Sasaki T, Chu ML, and Tsuda T (2016). Fibulin-2 is essential for angiotensin II-induced myocardial fibrosis mediated by transforming growth factor (TGF)-β. Lab. Invest 96, 773–783. [PubMed: 27111286]

Koeglsperger T, Li S, Brenneis C, Saulnier JL, Mayo L, Carrier Y, Selkoe DJ, and Weiner HL (2013). Impaired glutamate recycling and GluN2B-mediated neuronal calcium overload in mice lacking TGF-β1 in the CNS. Glia 61, 985–1002. [PubMed: 23536313]

Lai CP, Kim EY, Badr CE, Weissleder R, Mempel TR, Tannous BA, and Breakefield XO (2015). Visualization and tracking of tumour extracellular vesicle delivery and RNA translation using multiplexed reporters. Nat. Commun 6, 7029. [PubMed: 25967391]

Lee JE, Moon PG, Lee IK, and Baek MC (2015). Proteomic Analysis of Extracellular Vesicles Released by Adipocytes of Otsuka Long-Evans Tokushima Fatty (OLETF) Rats. Protein J. 34, 220–235. [PubMed: 25998041]

Levy AD, Omar MH, and Koleske AJ (2014). Extracellular matrix control of dendritic spine and synapse structure and plasticity in adulthood. Front. Neuroanat 8, 116. [PubMed: 25368556]

Luarte A, Henzi R, Fernández A, Gaete D, Cisternas P, Pizarro M, Batiz LF, Villalobos I, Masalleras M, Vergara R, et al. (2020). Astrocyte-Derived Small Extracellular Vesicles Regulate Dendritic Complexity through miR-26a-5p Activity. Cells 9, 930.

Maas SLN, Breakefield XO, and Weaver AM (2017). Extracellular Vesicles: Unique Intercellular Delivery Vehicles. Trends Cell Biol. 27, 172–188. [PubMed: 27979573]

McKenzie AJ, Hoshino D, Hong NH, Cha DJ, Franklin JL, Coffey RJ, Patton JG, and Weaver AM (2016). KRAS-MEK Signaling Controls Ago2 Sorting into Exosomes. Cell Rep. 15, 978–987. [PubMed: 27117408]

Mishra S, Wu SY, Fuller AW, Wang Z, Rose KL, Schey KL, and Mchaourab HS (2018). Loss of αB-crystallin function in zebrafish reveals critical roles in the development of the lens and stress resistance of the heart. J. Biol. Chem 293, 740–753. [PubMed: 29162721]

Murphy-Ullrich JE, and Poczatek M (2000). Activation of latent TGF-beta by thrombospondin-1: mechanisms and physiology. Cytokine Growth Factor Rev. 11, 59–69. [PubMed: 10708953]

Ono RN, Sengle G, Charbonneau NL, Carlberg V, Bächinger HP, Sasaki T, Lee-Arteaga S, Zilberberg L, Rifkin DB, Ramirez F, et al. (2009). Latent transforming growth factor beta-binding proteins and fibulins compete for fibrillin-1 and exhibit exquisite specificities in binding sites. J. Biol. Chem 284, 16872–16881. [PubMed: 19349279]

Papa M, Bundman MC, Greenberger V, and Segal M (1995). Morphological analysis of dendritic spine development in primary cultures of hippocampal neurons. J. Neurosci 15, 1–11. [PubMed: 7823120]

Pascua-Maestro R, González E, Lillo C, Ganfornina MD, Falcón-Pérez JM, and Sanchez D (2019). Extracellular Vesicles Secreted by Astroglial Cells Transport Apolipoprotein D to Neurons and Mediate Neuronal Survival Upon Oxidative Stress. Front. Cell. Neurosci 12, 526. [PubMed: 30687015]

Radice PD, Mathieu P, Leal MC, Farias MI, Ferrari C, Puntel M, Salibe M, Chernomoretz A, and Pitossi FJ (2015). Fibulin-2 is a key mediator of the pro-neurogenic effect of TGF-beta1 on adult neural stem cells. Mol. Cell. Neurosci 67, 75–83. [PubMed: 26051800]

Sasaki T, Göhring W, Pan TC, Chu ML, and Timpl R (1995). Binding of mouse and human fibulin-2 to extracellular matrix ligands. J. Mol. Biol 254, 892–899. [PubMed: 7500359]

Schaeffer J, Tannahill D, Cioni JM, Rowlands D, and Keynes R (2018). Identification of the extracellular matrix protein Fibulin-2 as a regulator of spinal nerve organization. Dev. Biol 442, 101–114. [PubMed: 29944871]

Shelke GV, Yin Y, Jang SC, Lässer C, Wennmalm S, Hoffmann HJ, Li L, Gho YS, Nilsson JA, and Lötvall J (2019). Endosomal signalling via exosome surface TGFβ-1. J. Extracell. Vesicles 8, 1650458. [PubMed: 31595182]

Shi M, Majumdar D, Gao Y, Brewer BM, Goodwin CR, McLean JA, Li D, and Webb DJ (2013). Glia co-culture with neurons in microfluidic platforms promotes the formation and stabilization of synaptic contacts. Lab Chip 73, 3008–3021.

Singh SK, Stogsdill JA, Pulimood NS, Dingsdale H, Kim YH, Pilaz LJ, Kim IH, Manhaes AC, Rodrigues WS Jr., Pamukcu A, et al. (2016). Astrocytes Assemble Thalamocortical Synapses by Bridging NRX1α and NL1 via Hevin. Cell 164, 183–196. [PubMed: 26771491]

Song I, and Dityatev A (2018). Crosstalk between glia, extracellular matrix and neurons. Brain Res. Bull 136, 101–108. [PubMed: 28284900]

Sung BH, and Weaver AM (2017). Exosome secretion promotes chemotaxis of cancer cells. Cell Adhes. Migr 11, 187–195.

Tang CZ, Yang JT, Liu QH, Wang YR, and Wang WS (2019). Up-regulated miR-192-5p expression rescues cognitive impairment and restores neural function in mice with depression via the Fbln2-mediated TGF-β1 signaling pathway. FASEB J. 33, 606–618. [PubMed: 30118321]

Théry C, Witwer KW, Aikawa E, Alcaraz MJ, Anderson JD, Andriantsitohaina R, Antoniou A, Arab T, Archer F, Atkin-Smith GK, et al. (2018). Minimal information for studies of extracellular vesicles 2018 (MISEV2018): a position statement of the International Society for Extracellular Vesicles and update of the MISEV2014 guidelines. J. Extracell. Vesicles 7, 1535750. [PubMed: 30637094]

Timpl R, Sasaki T, Kostka G, and Chu ML (2003). Fibulins: a versatile family of extracellular matrix proteins. Nat. Rev. Mol. Cell Biol 4, 479–489. [PubMed: 12778127]

Ullian EM, Sapperstein SK, Christopherson KS, and Barres BA (2001). Control of synapse number by glia. Science 297, 657–661.

Varcianna A, Myszczynska MA, Castelli LM, O'Neill B, Kim Y, Talbot J, Nyberg S, Nyamali I, Heath PR, Stopford MJ, et al. (2019). Micro-RNAs secreted through astrocyte-derived extracellular vesicles cause neuronal network degeneration in C9orf72 ALS. EBioMedicine 40, 626–635. [PubMed: 30711519]

Voss BJ, Loh JT, Hill S, Rose KL, McDonald WH, and Cover TL (2015). Alteration of the Helicobacter pylori membrane proteome in response to changes in environmental salt concentration. Proteomics Clin. Appl 9, 1021–1034. [PubMed: 26109032]

Wang S, Cesca F, Loers G, Schweizer M, Buck F, Benfenati F, Schach-ner M, and Kleene R (2011). Synapsin I is an oligomannose-carrying glycoprotein, acts as an oligomannose-binding lectin, and promotes neurite outgrowth and neuronal survival when released via glia-derived exosomes. J. Neurosci 37, 7275–7290.

Wang G, Dinkins M, He Q, Zhu G, Poirier C, Campbell A, Mayer-Proschel M, and Bieberich E (2012). Astrocytes secrete exosomes enriched with proapoptotic ceramide and prostate apoptosis response 4 (PAR-4): potential mechanism of apoptosis induction in Alzheimer disease (AD). J. Biol. Chem 287,21384–21395. [PubMed: 22532571]

Webber J, Steadman R, Mason MD, Tabi Z, and Clayton A (2010). Cancer exosomes trigger fibroblast to myofibroblast differentiation. Cancer Res 70, 9621–9630. [PubMed: 21098712]

Wegner AM, Nebhan CA, Hu L, Majumdar D, Meier KM, Weaver AM, and Webb DJ (2008). N-wasp and the arp2/3 complex are critical regulators of actin in the development of dendritic spines and synapses. J. Biol. Chem 283, 15912–15920. [PubMed: 18430734]

Xu J, Xiao N, and Xia J (2010). Thrombospondin 1 accelerates synaptogenesis in hippocampal neurons through neuroligin 1. Nat. Neurosci 13, 22–24. [PubMed: 19915562]

You Y, Borgmann K, Edara VV, Stacy S, Ghorpade A, and Ikezu T (2019). Activated human astrocyte-derived extracellular vesicles modulate neuronal uptake, differentiation and firing. J. Extracell. Vesicles 9, 1706801. [PubMed: 32002171]

Yu K, Ge J, Summers JB, Li F, Liu X, Ma P, Kaminski J, and Zhuang J (2008). TSP-1 secreted by bone marrow stromal cells contributes to retinal ganglion cell neurite outgrowth and survival. PLoS ONE 3, e2470. [PubMed: 18575624]

Zhang H, Wu J, Dong H, Khan SA, Chu ML, and Tsuda T (2014). Fibulin-2 deficiency attenuates angiotensin II-induced cardiac hypertrophy by reducing transforming growth factor-β signalling. Clin. Sci. (Lond.) 126, 275–288. [PubMed: 23841699]

Highlights

- Astrocyte-derived small EVs (SEVs) enhance neuronal spine and synapse formation
- Fibulin-2 is a key synaptogenic cargo present on astrocyte-derived SEVs
- Astrocyte SEVs and fibulin-2 activate TGF-β signaling in neurons
- Astrocyte SEV- and fibulin-2-driven synaptogenesis depend on TGF-β signaling

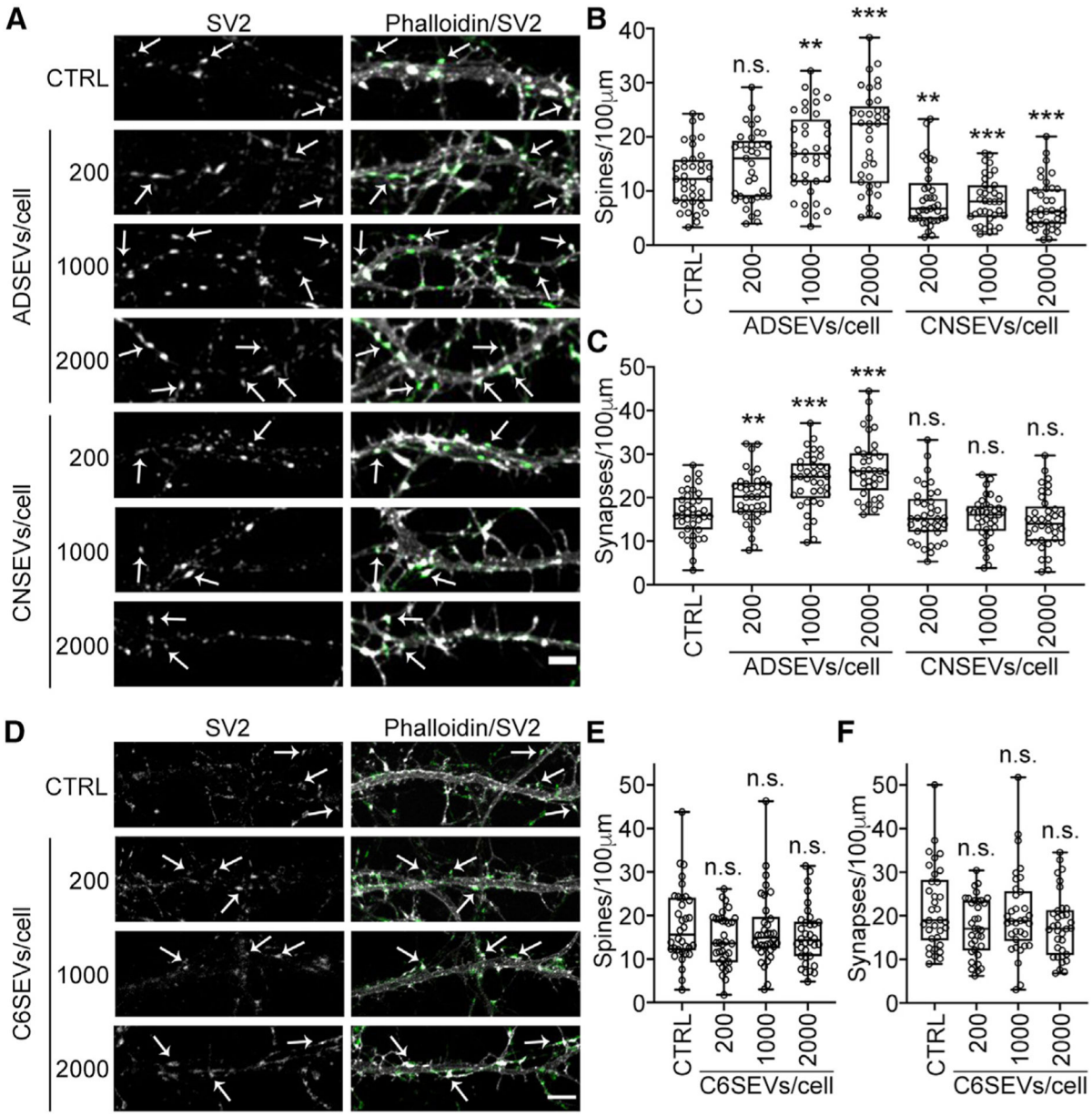

Figure 1. Astrocyte-derived SEVs promote dendritic spine and synapse formation

(A and D) Representative fluorescence images of dendrites in day 12 neurons treated for 48 h with 0 (control), 200, 1,000, or 2,000 astrocyte-derived (ADSEVs), cortical neuron-derived (CNSEVs), or C6 glioma-derived (C6SEVs) SEVs /neuron. Images in (A) and (D) are adjusted for brightness and contrast and cropped to same size using Fiji for better visualization of SV2 colocalization on dendritic spines. Left panel: SV2 only. Right panel: overlay of phalloidin (grayscale) and SV2 (green). Example dendritic spines are indicated with arrows. Scale bars, 5 μm. (B, C, E, and F) Quantification of spine and synapse density from images. n ≥ 36 primary or secondary dendrites from 3 independent experiments. Data represented as box and whiskers plots with all data points shown, bar indicating the median, and the box showing interquartile range. **p < 0.01, ***p < 0.001; n.s., not significant.

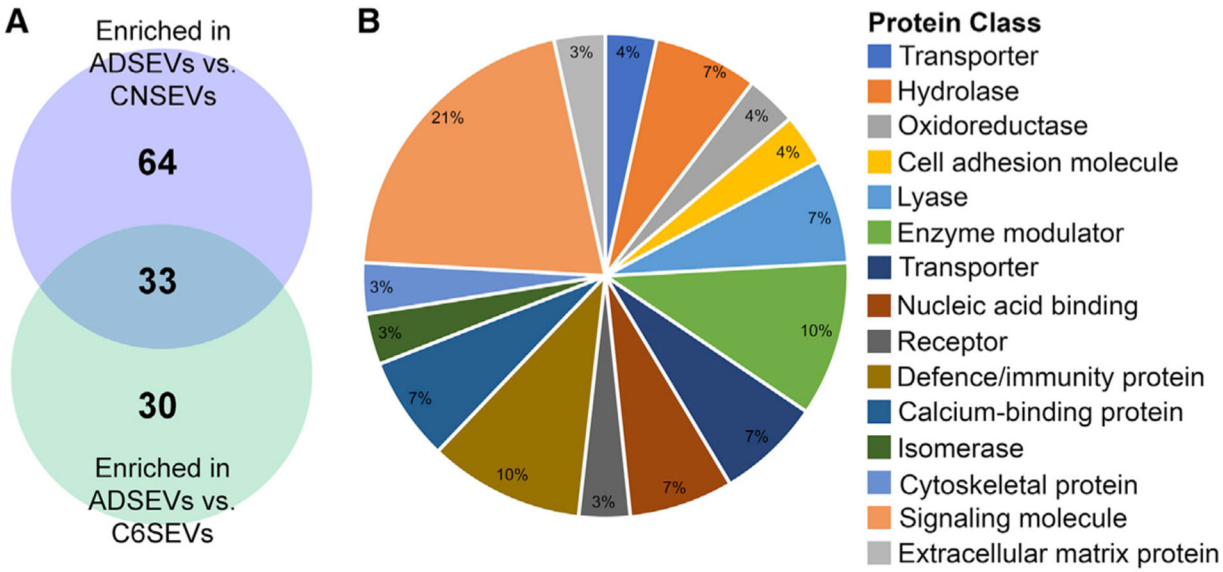

C

Protein name	Fold change compared to	
	C6-SEVs	CN-SEVs
Collagen alpha-1(I) chain	8.65	8.50
Alpha-2-macroglobulin	8.57	9.03
Microfibril-associated glycoprotein 4-like	7.76	12.04
Fibulin 2	6.64	5.29
Protein S100-A6	6.03	13.53
Epoxide hydrolase 1	5.86	4.29
Atrial natriuretic peptide receptor 3	5.80	5.00
Low-density lipoprotein receptor-related protein 2	5.77	4.04
Tubulin tyrosine ligase-like 12	5.51	6.25
Annexin A3	5.37	3.97
Complement C3	5.09	7.49
Coiled-coil domain-containing 150	5.08	5.96

Figure 2. Identification of enriched astrocyte SEV proteins using quantitative comparative proteomics

(A) Venn diagram of proteins enriched in ADSEVs compared to CNSEVs and C6SEVs identified by iTRAQ proteomics analysis. n = 1

(B) Classification of 33 proteins from the overlap in (A) represented as the pie chart based on protein class.

(C) List of 12 proteins significantly higher in ADSEVs compared to C6SEVs out of the 33 enriched proteins.

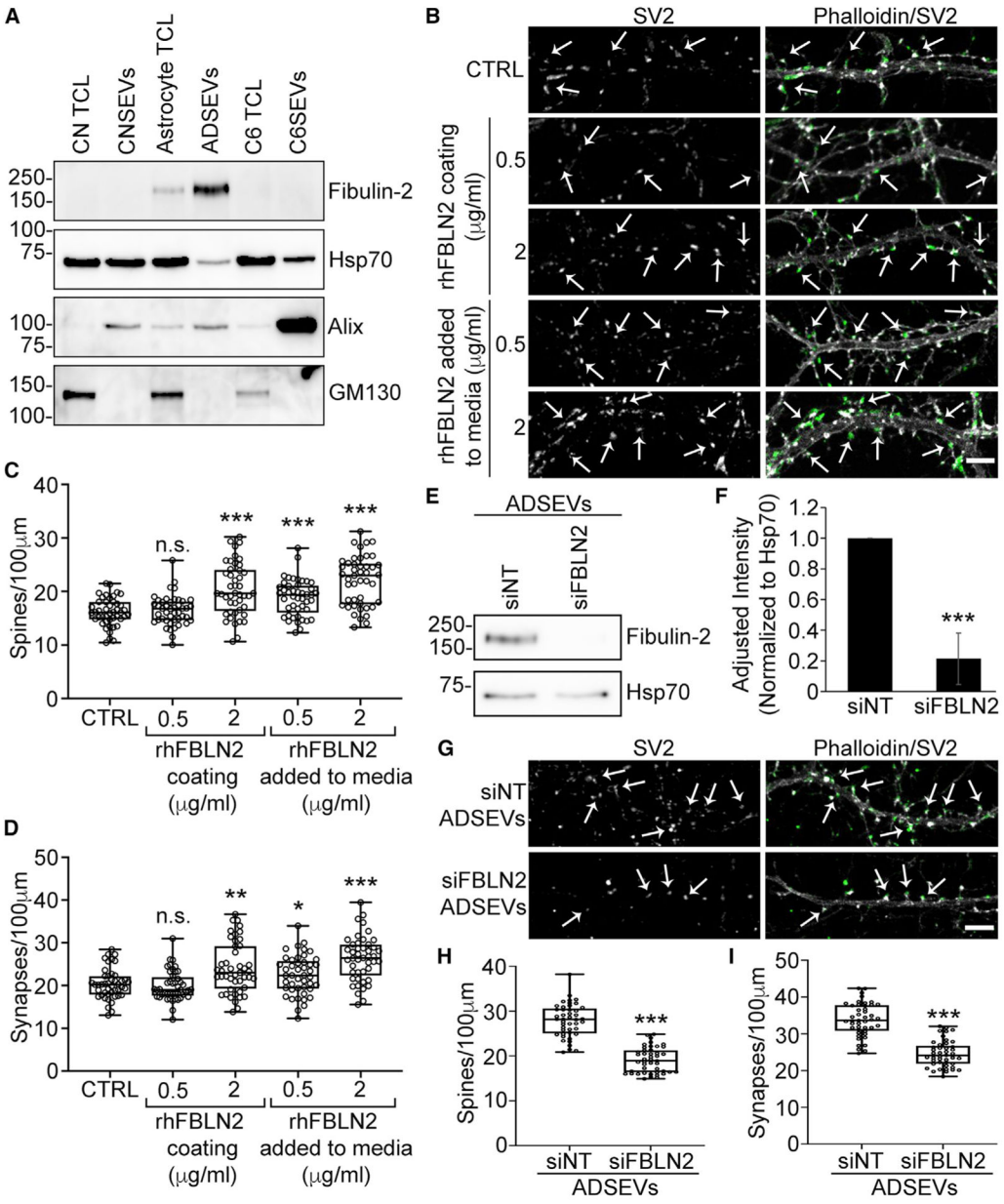

Figure 3. Fibulin-2 is a synaptogenic cargo present in astrocyte SEVs

(A) Western blot of equal protein (10 μg) of cortical neurons, astrocytes and C6 total cell lysates (TCLs) and SEVs stained for fibulin-2, the SEV markers Hsp70 and Alix, or the Golgi marker GM130. n = 3 (quantification in Figure S2E).

(B) Representative images from day 12 cortical neurons plated on coverslips coated with poly-D-Lysine (control) in the presence or absence of soluble recombinant human fibulin-2 (rhFBLN2) added to media or plated on coverslips coated with rhFBLN2 for 48 h. Scale bar, 5 μm.

(C and D) Quantification of spines and synapses from images. n = 45 primary or secondary dendrites from 3 independent experiments.

(E) Representative western blot of control (siNT) and fibulin-2 knockdown (siFBLN2) ADSEVs stained for fibulin-2 and SEV marker Hsp70.
(F) Quantification of fibulin-2 levels in siNT and siFBLN2 ADSEVs. n = 3. Data are normalized to Hsp70 levels and represented as mean ± SEM.
(G) Representative images of day 12 neuronal dendrites treated for 48 h with 2,000 siNT/siFBLN2 ADSEVs per neuron. Images in (B) and (G) are adjusted for brightness and contrast and cropped to same size using Fiji for better visualization of SV2 colocalization on dendritic spines. Left panel: SV2 only. Right panel: overlay of phalloidin in grayscale and SV2 in green. Example dendritic spines are indicated with arrows. Scale bar, 5 μm.
(H and I) Quantification of spine and synapse density from images. n = 45 primary or secondary dendrites from 3 independent experiments. Data represented as box and whiskers plots with all data points shown, bar indicating the median, and the box showing interquartile range. *$p < 0.05$, **$p < 0.01$, ***$p < 0.001$; n.s., not significant.

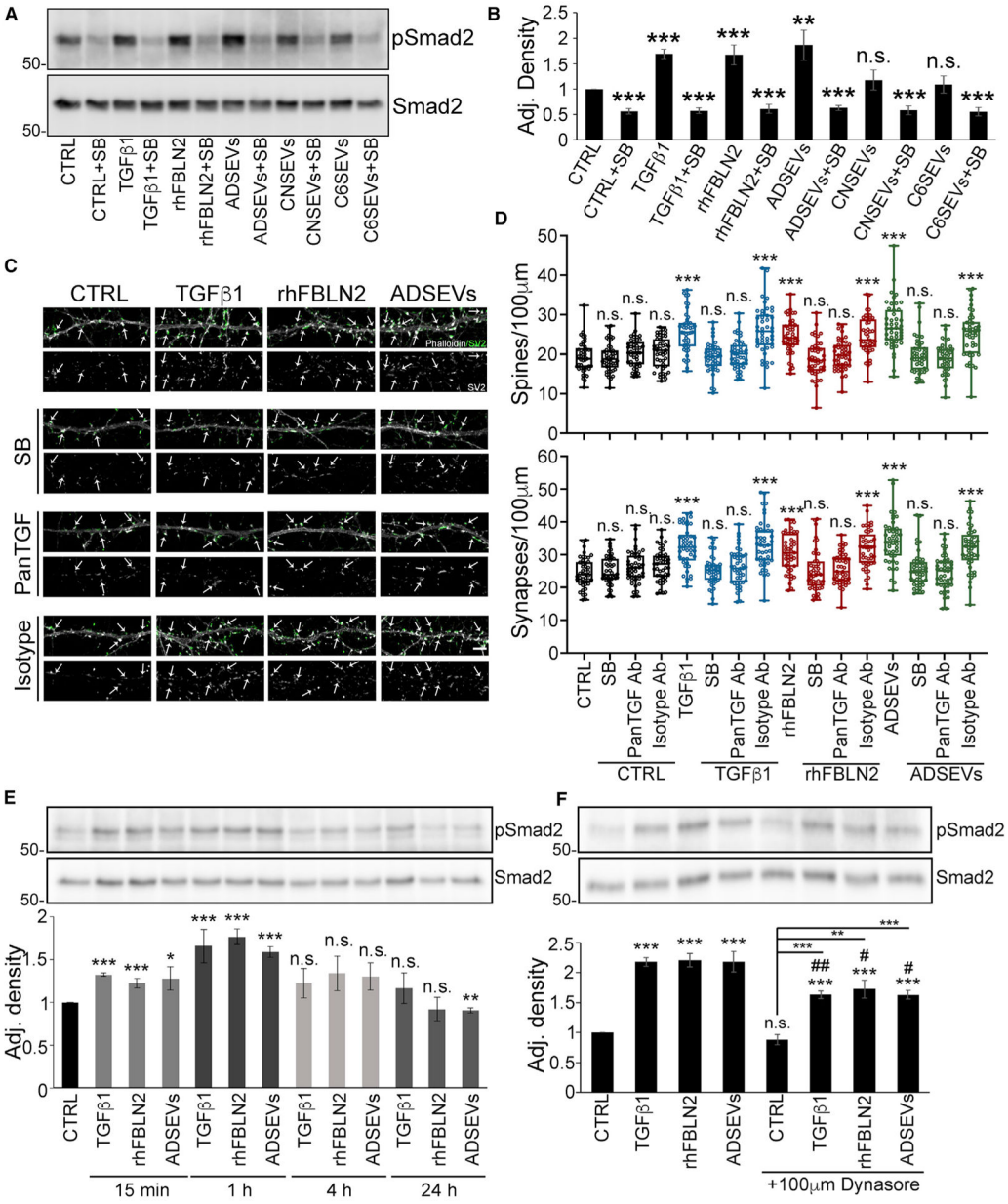

Figure 4. Astrocyte-derived SEVs and fibulin-2 activate TGF-β signaling to increase spine and synapse formation

(A and B) Cortical neurons were treated with 10 ng/mL TGF-β1, 2 μg/mL rhFBLN2, or 2,000 SEVs/cell, as indicated, for 1 h in the absence or presence of 10 μM SB431542 (SB) before lysis and western blot analysis for phospho-Smad2 and total Smad2. (A) Representative western blots. (B) Quantification of absolute density of pSmad2 levels compared to total Smad2 levels. n = 3. Data represented as mean ± SEM.

(C) Representative images of day 12 neurons treated with 10 ng/mL TGF-β1, 2 μg/mL rhFBLN2, or ADSEVs in the absence or presence of 2.5 μM SB, 10 μg/mL pan-TGFβ-neutralizing antibody or mouse IgG_1 isotype control antibody. Images are adjusted for brightness and contrast and cropped to same size using Fiji for better visualization of SV2

colocalization on dendritic spines. SV2 only in grayscale. Overlay of phalloidin in grayscale and SV2 in green. Example dendritic spines are indicated with arrows. Scale bar, 5 μm.
(D) Quantification of spines and synapses from images. n = 45 primary or secondary dendrites from 3 independent experiments. Data represented as box and whiskers plots with all data points shown, bar indicating the median, and the box showing interquartile range.
(E) Representative western blot images and quantification of pSmad2 levels compared to total Smad2 levels for cortical neurons treated with 10 ng/ml TGF-β1, 2 μg/ml recombinant human fibulin-2 or 2000 ADSEVs/cell for 15 min, 1 h, 4 h, and 24 h (n = 3). Data represented as mean ± SEM.
(F) Representative western blot images and quantification of pSmad2 levels compared to total Smad2 levels for cortical neurons treated with 10 ng/mLTGF-β1, 2 μg/mL recombinant human fibulin-2, or 2,000 ADSEVs/cell in the absence or presence of 100 μM Dynasore (n = 4). Data represented as mean ± SEM # indicates comparison between same condition in the absence or presence of Dynasore. #/*p < 0.05, ##/**p < 0.01, ***p < 0.001; n.s., not significant.

KEY RESOURCES TABLE

REAGENT or RESOURCE	SOURCE	IDENTIFIER
Antibodies		
Mouse monoclonal anti-SV2	Developmental Studies Hybridoma Bank, University of Iowa, Iowa City, IA	Cat# SV2; RRID:AB_2315387
Mouse monoclonal anti-PSD95	Millipore Sigma	Cat# MAB1598; RRID:AB_94278
Alexa Fluor 647 Goat Anti-mouse IgG	Molecular Probes	Cat# A-21236; RRID:AB_141725
Rabbit polyclonal anti-TSG101	Abcam	Cat# ab30871; RRID:AB_2208084
Mouse monoclonal anti-Flotillin-1	BD Biosciences	Cat# 610820; RRID:AB_398139
Mouse monoclonal anti-Hsp70	Santa Cruz Biotechnology	Cat# sc-24; RRID:AB_627760
Mouse monoclonal anti-Alix	Cell Signaling	Cat# 2171; RRID:AB_2299455
Mouse monoclonal anti-GM130	BD Biosciences	Cat# 610822; RRID:AB_398141
Rabbit polyclonal anti-α2M	Abcam	Cat# ab58703; RRID:AB_879541
Rabbit monoclonal anti-Vimentin	Cell Signaling	Cat# 5741; RRID:AB_10695459
Rabbit polyclonal anti-Connexin 43	Cell Signaling	Cat# 3512; RRID:AB_2294590
Rabbit polyclonal anti-Integrin α6	Cell Signaling	Cat# 3750; RRID:AB_2249263
HRP conjugated goat anti-mouse IgG	Promega	Cat# W4021; RRID:AB_430834
HRP conjugated goat anti-rabbit IgG	Promega	Cat# W4011; RRID:AB_430833
Rabbit polyclonal anti-Fibulin-2	GeneTex	Cat# GTX105108; RRID:AB_2036908
Rabbit polyclonal anti-GFAP	Bioss	Cat# bs-0199R; RRID: AB_10859014
Rabbit monoclonal anti-Phospho-Smad2	Cell Signaling	Cat# 3108; RRID:AB_490941
Rabbit monoclonal anti-Smad2	Cell Signaling	Cat# 5339; RRID:AB_10626777
Mouse monoclonal anti-TGFbeta1,2,3	R&D Systems	Cat# MAB1835; RRID:AB_1672402
Normal mouse IgG_1	Santa Cruz Biotechnology	Cat# sc-3877; RRID:AB_737222
Chemicals, peptides, and recombinant proteins		
Neurobasal™ Medium	GIBCO	Cat# 21103-049
B-27 Supplement (50x), serum free	GIBCO	Cat# 17504-044
Minimum Essential Medium	Corning	Cat# 10-010-CV
Ham's F-12K (Kaighn's) Medium	GIBCO	Cat# 21-127-022
DNase I	Sigma-Aldrich	Cat# DN25-100MG
HBSS (10x), no calcium, no magnesium, no phenol red	GIBCO	Cat# 14-185-052
Horse Serum	GIBCO	Cat# 16-050-122
Trypsin (2.5%), no phenol red	GIBCO	Cat# 15-090-046
Poly-D-lysin hydrobromide	Sigma-Aldrich	Cat# P7886-50MG
Alexa Fluor™ 488 Phalloidin	Molecular Probes	Cat# A12379
Aqua-Poly/Mount	Polysciences Inc	Cat# 18606
Recombinant Human Fibulin 2 Protein	R&D Systems	Cat# 9559-FB-050
Recombinant Human TGF-beta 1 Protein	R&D Systems	Cat# 240-B-002
SB 431542 hydrate	Sigma-Aldrich	Cat# S4317-5MG
Dynamin Inhibitor I, Dynasore	Sigma-Aldrich	Cat# 32441-10MG
FM4-64FX	Invitrogen	Cat# F34653

REAGENT or RESOURCE	SOURCE	IDENTIFIER
Transferrin, AF 546 Conjugate	Thermo Scientific	Cat# T23364
Complete Tablets, Mini Protease Inhibitor Cocktail Tablets	Roche	Cat# 04-693-124-001
PhosSTOP Phosphatase Inhibitor Cocktail Tablets	Roche	Cat# 04-906-837-001
Pierce™ ECL Western Blotting Substrate	Thermo Scientific	Cat# 32106
Supersignal™ West Femto Maxium Sensitivity Substrate	Thermo Scientific	Cat# 34095
X-tremeGENE™ siRNA transfection reagent	Millipore Sigma	Cat# 4476093001
Experimental models: cell lines		
Rat: C6 glioma cell line	Kindly provided by Dr. James G. Patton, Vanderbilt University, USA	N/A
Experimental models: organisms/strains		
Rat: SAS SD-Rat Female Timed Preg-Day 18	Charles River Laboratories	Strain: 24104855
Oligonucleotides		
Non-targeting siRNAs pool UGGUUUACAUGUCGACUAA, UGGUUUACAUGUUGUGUGA, UGGUUUACAUGUUUUCUGA, UGGUUUACAUGUUUUCCUA	Dharmacon	Cat# D-001810-10-20
Rat Fbln2 siRNAs -SMARTpool CGGCAGGUGUGUCGCGUUA, CAAUGAGUGCACAUCGUUA, CCAAUAGCCUGCCGGGAGA, AUGAUCAAAUAGCACGAAA	Dharmacon	Cat# L-095315-02-0050
Software and algorithms		
Prism 8	GraphPad Prism	RRID:SCR_002798
MetaMorph	MetaMorph Microscopy Automation and Image Analysis Software	RRID:SCR_002368
NIS-Elements	Nikon	RRID:SCR_014329
Fiji	Fiji	RRID:SCR_002285
ImageStudioLite version 5.2.5	LiCOR	RRID:SCR_013715
BioRender	BioRender	https://biorender.com
Other		
Falcon® Cell strainer 70 μm Nylon	Corning	Cat# 352350